Pressure-Induced Emission Enhancement in 2-(anthracen-9-yl)-9H-thioxanthen-9-one Crystals with π-π Stacked Thioxanthone Dimers

Ming Wang, Daojie Yang, Yonghui Lv, Haichao Liu, Kai Wang,* and Yuxiang Dai,**

Department of Materials Physics and Chemistry, School of Materials Science and Engineering, Northeastern University, Shenyang, 110819, China.

State Key Laboratory of Supramolecular Structure and Materials, College of Chemistry, Jilin University, Changchun, 130012, China.

School of Physics Science and Information Technology, Shandong Key Laboratory of Optical Communication Science and Technology, Liaocheng University, Liaocheng, Shandong, 252000, P. R. China.

Email: daiyuxiang@mail.neu.edu.cn

Experimental section

All reagents and solvents were used as received from commercial suppliers. Characterization was performed via NMR (Bruker AVANCE 500, TMS standard), mass spectrometry (Thermo Fisher ITQ1100), and elemental analysis (Flash EA 1112). Synthetic procedures are detailed in the Supporting Information.

Single crystal X-ray diffraction (SCXRD) data

Single crystals of TXAN were grown at room temperature by solvent diffusion in a dichloromethane-methanol system. Diffraction data were collected on a Rigaku R-AXIS RAPID diffractometer (Mo-Kα) using RAPID AUTO, and the structure was solved by direct methods and refined by full-matrix least-squares with OLEX2.

Photophysical measurements

Using an Edinburgh FLS980 spectrometer, steady-state emission spectra of TXAN were recorded in tetrahydrofuran (THF)-water mixed solutions, time-resolved emission spectra of crystals were collected via time-correlated single photon counting (TSCPC), and photoluminescence quantum yields of crystals under ambient conditions were measured with the integrating sphere accessory.

Determination of photoluminescence quantum yield

The PLQY, k_{nr} and k_r were calculated using the following equation:

$$\Phi = \Phi_0 \times \frac{I}{I_0} \times \frac{A_0(\lambda_{ex})}{A(\lambda_{ex})} \times \frac{n^2}{{n_0}^2},$$

(Φ_0 is the PLQY at ambient pressure, I/I_0 is the normalized integral ratio of emission intensity, $A(\lambda_{ex})/A_0(\lambda_{ex})$ is the absorption ratio at the excitation wavelength, and n^2/n_0^2 is the ratio of the squares of the refractive indices.)

$$\Phi = \frac{k_r}{(k_r + k_{nr})}$$

$$\tau = \frac{1}{(k_r + k_{nr})}$$

(radiative transition rate k_r and non-radiative transition rate k_{nr}).

High-pressure measurements

In situ high-pressure experiments were carried out at room temperature using a symmetric diamond anvil cell (DAC, 400 μm culet diamonds). TXAN crystals were placed in a ~150 μm-diameter hole of a T301 stainless-steel gasket pre-indented to 40 μm, with pressure determined by the ruby R1 fluorescence spectrum.[1] For high-pressure PL and UV-vis absorbance experiments, silicon oil (Aldrich) served as the pressure transmitting medium (PTM), whereas KBr was used for IR measurements. High-pressure PL was measured with an optical fiber spectrometer (Ocean Optics, QE6500) under 355 nm UV DPSS laser excitation, while X-ray diffraction studies of TXAN crystals were performed at the BL15U1 beamline of SSRF, and the stacking structure of the derivatives was subsequently analyzed using Mercury software.

High-pressure geometric optimization

Ab initio calculations of the high-pressure crystal structure were performed by using the pseudopotential plane wave method in the CASTEP package.[2] The generalized gradient approximation of Perdew-Burke-Ernzerh exchange correlation was used in the geometric optimization with a plane wave cutoff energy of 700 eV.[3]

Theoretical calculation

Based on the TXAN crystal geometry, TD-DFT calculations at the B3LYP/6-31G(d, p) level were performed using Gaussian 16 (Rev. C.01) on a Power Leader

cluster to determine the natural transition orbitals (NTOs) of the lowest excited singlet state (S_1).[4]

Synthetic details

Synthesis of 2-(anthracen-9-yl)-9H-thioxanthen-9-one (TX-AN)

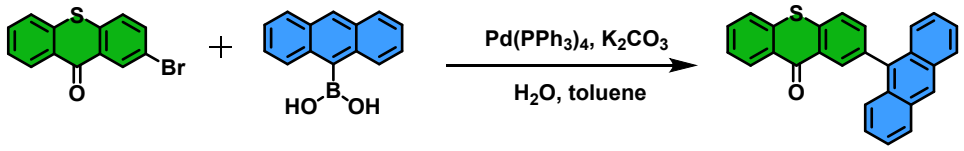

TX-Br **AN-B** **TXAN**

A mixture of 2-bromo-9H-thioxanthen-9-one (TX-Br, 815.25 mg, 2.80 mmol), anthracen-9-ylboronic acid (AN-B, 555.13 mg, 2.50 mmol), K_2CO_3 (3317.04 mg, 24.00 mmol), 12 mL distilled water, and 18 mL toluene was degassed and recharged with nitrogen. Then $Pd(PPh_3)_4$ (92.45 mg, 0.08 mmol) was added in the mixture as catalyst, and the mixture was degassed and recharged with nitrogen again. After stirred and refluxed at 90 ℃ for 48 h under nitrogen atmosphere, the mixture was extracted with dichloromethane. The organic phase was dried with anhydrous sodium sulfate, filtered and concentrated in vacuum. It was purified via silica gel chromatography by the mixture of petroleum ether/dichloromethane (2:1) to afford the desired compound in 60% yield (580 mg). ^{1}H NMR (500 MHz, CD_2Cl_2, 25 ℃, TMS): δ 8.70 (s, 1H), 8.67 – 8.61 (m, 2H), 8.14 (d, *J* = 8.5 Hz, 2H), 7.90 (d, *J* = 8.1 Hz, 1H), 7.80 – 7.72 (m, 3H), 7.68 (d, *J* = 8.8 Hz, 2H), 7.62 – 7.56 (m, 1H), 7.54 (t, *J* = 7.5 Hz, 2H), 7.45 – 7.38 (m, 2H). ^{13}C NMR (126 MHz, CD_2Cl_2, 25 ℃, TMS): δ 179.62, 137.23, 137.01, 136.58, 135.34, 135.16, 132.42, 132.11, 131.38, 130.24, 129.68, 129.40, 129.35, 128.43, 127.14, 126.46, 126.34, 126.26, 126.21, 125.76, 125.23. GC/MS, EI (mass *m/z*): 388.40

$[M]^+$ (calcd: 388.48). Molecular formula $C_{27}H_{16}OS$ requires C, 83.48; H, 4.15; O, 4.12; S, 8.25; Found: C, 83.50; H, 4.23; S, 8.42.

Table S1. Crystallographic data and refinement data of **TXAN** crystals.

	TXAN
crystal color	colorless
empirical formula	$C_{27}H_{16}OS$
formula weight	388.46
***T* [K]**	302(2)
crystal system	monoclinic
space group	C 2/c
***a* [Å]**	30.900(4)
***b* [Å]**	7.5662(9)
***c* [Å]**	18.161(2)
***α* [°]**	90
***β* [°]**	114.090(9)
***γ* [°]**	90
***V* [Å^3]**	3876.2(9)
Z	8
F(000)	1616
Density [g/cm^3]	1.331
***μ* [mm^{-1}]**	0.183
Reflections collected	31047
Unique reflections	3401
***R* (int)**	0.0880
GOF	1.020
R_1 [$I>2\sigma(I)$]	0.0654
ωR_2 [$I>2\sigma(I)$]	0.1429
R_1 (all data)	0.0961
ωR_2 (all data)	0.1607
CCDC number	2521451

Table S2. Photoluminescence quantum yield (PLQY) and lifetimes (τ), radiative recombination rate (K_r) and non-radiative recombination rate (K_{nr}) of TXAN in different solvents.

	HEX	ETE	THF	ACN
PLQY(%)	0.01	0.45	2.59	0.78
τ(ns)	0.37744	0.43495	4.05017	3.73744
$K_r(ns^{-1})$	0.00026	0.01034	0.00639	0.00208
$K_{nr}(ns^{-1})$	2.64916	2.28876	0.24051	0.26548

Table S3. Pressure-dependence of PLQY evolution of TXAN crystals.

Pressure (GPa)	**PL integral intensity I/I_0**	**Cell volume V/V_0**	**Refractive Index square n^2**	**n^2/n_0^2**	**PLQY(%)**
0	1	1	2.4649	1	0.66
0.31	1.31521	0.96718	2.51339	1.01967	0.84462
0.63	1.28465	0.94128	2.57694	1.04545	0.83863
0.95	1.15519	0.92369	2.62321	1.06422	0.80820
1.91	0.97088	0.88458	2.73655	1.11021	0.55370
3.04	0.79190	0.84800	2.85782	1.15940	0.31765
4.01	0.60753	0.83235	2.91505	1.18262	0.19639
5.06	0.43502	0.80891	3.00768	1.22020	0.17899

Table S4. Pressure-dependence of TXAN lifetime, radiative recombination rate and non-radiative recombination rate.

Pressure (GPa)	**K_r (ns^{-1})**	**K_{nr} (ns^{-1})**	**τ (ns)**
0	0.01539	2.31713	0.42872
0.31	0.01683	1.97525	0.50199
0.63	0.01314	1.55317	0.63845
0.95	0.01308	1.60515	0.61796
1.91	0.00989	1.77595	0.55996
3.04	0.00629	1.97479	0.50478
4.01	0.00411	2.08941	0.47766
5.06	0.00392	2.18799	0.45622

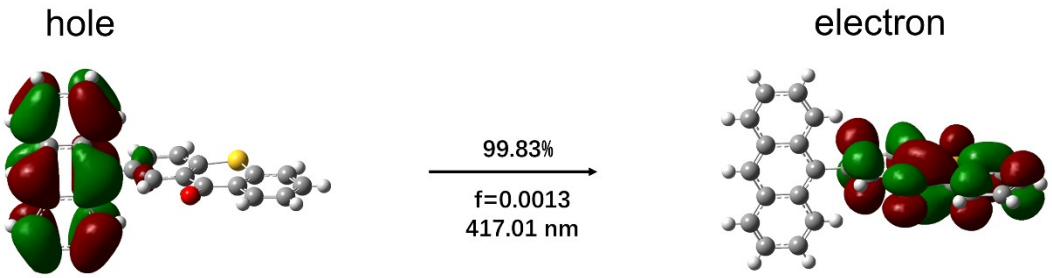

Fig. S1. NTO analysis of the TXAN molecule.

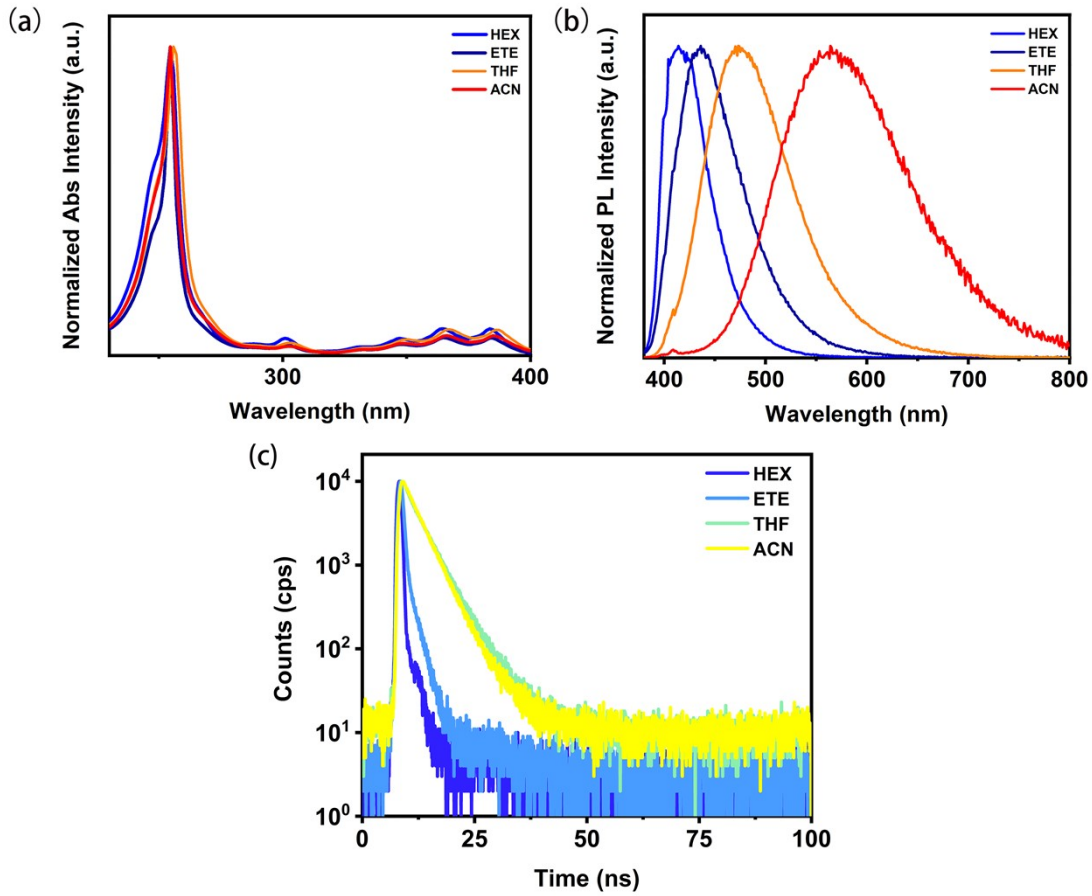

Figure S2. (a) UV–Vis absorption spectra of TXAN in different solvents. (b) PL spectra of TXAN in different solvents. (c) Plots of fluorescence lifetime for TXAN in different solvents. HEX is hexane, ETE is ethyl ether, THF is tetrahydrofuran, and ACN is acetonitrile.

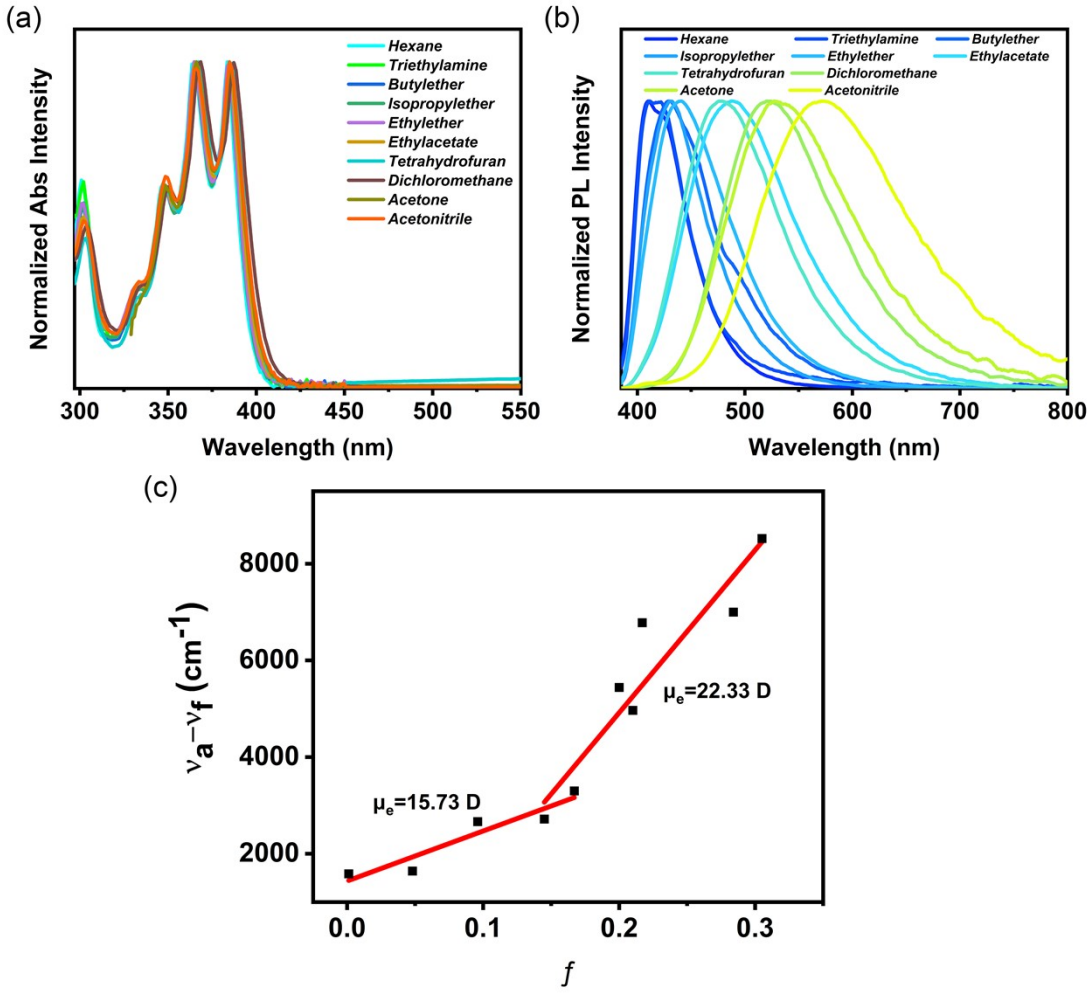

Figure S3. (a)Absorption spectra of TXAN in solvents of varying polarity. (b) Emission spectra of TXAN in solvents of varying polarity. (c) Linear correlation of the orientation polarization (f) of solvent media with the Stokes shift (ν_a-ν_f) for TXAN.

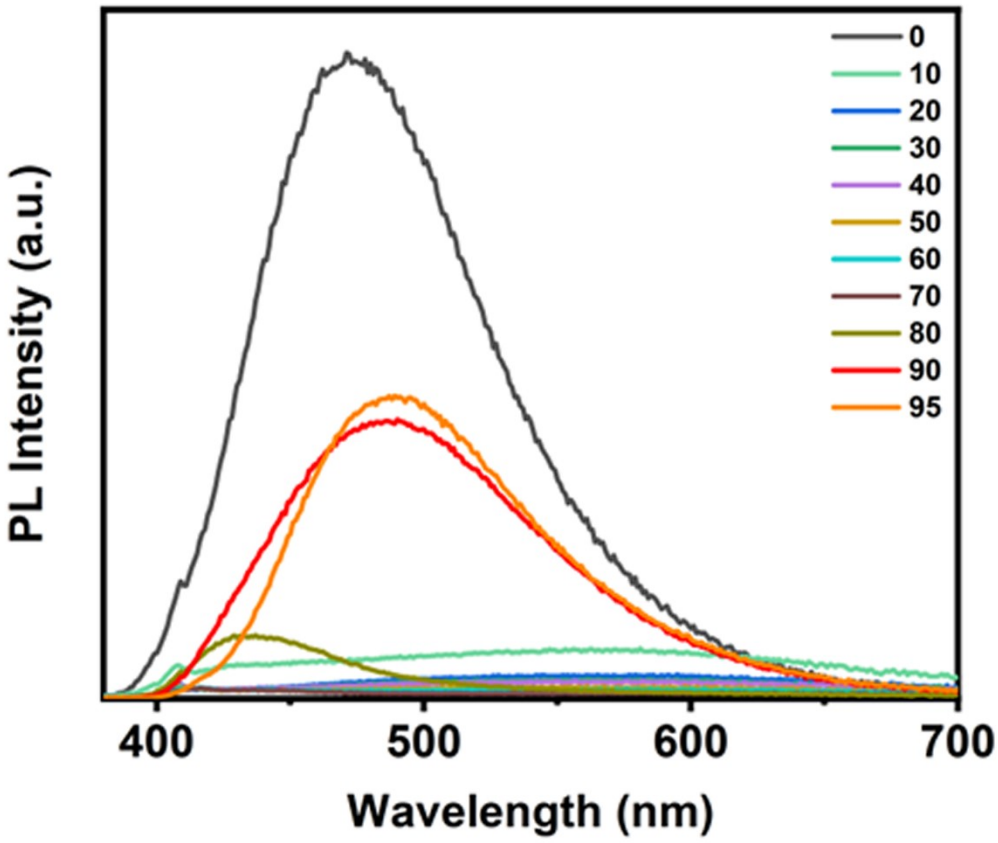

Figure S4. PL spectra of TXAN in mixed water/THF solutions with various water fractions(f_ω).

(The illustration shows Photographs of TXAN in mixed water/THF solutions under 365 nm UV lamp irradiation.)

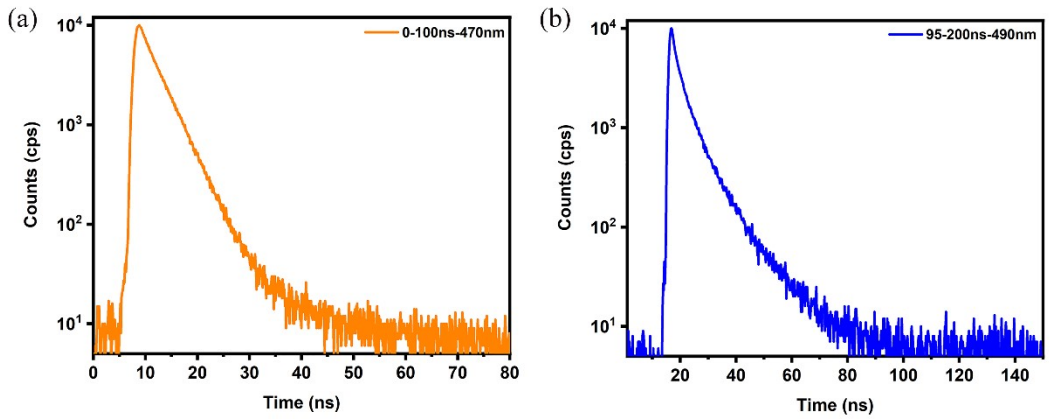

Figure S5. (a) PL decay curves of TXAN in mixed f_{ω}=0% water/THF solutions.

(b) PL decay curves of TXAN in mixed f_{ω}=95% water/THF solutions.

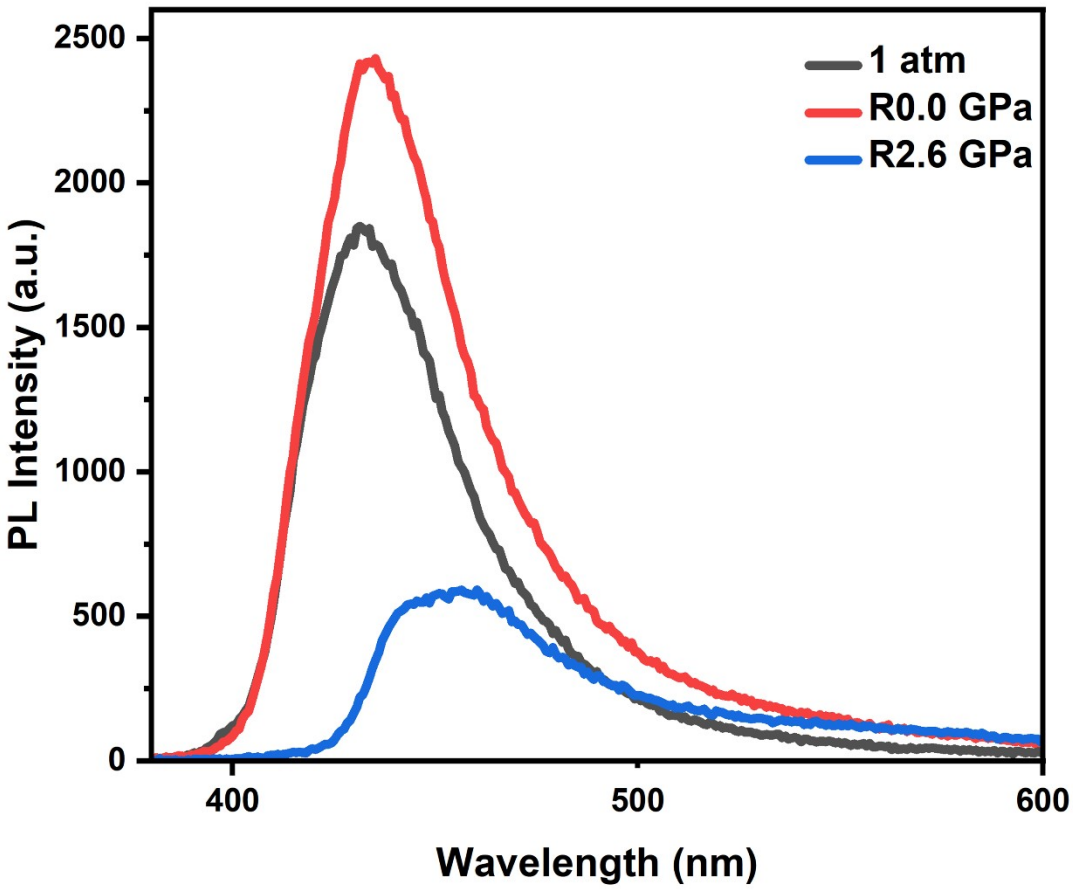

Figure S6. Selected PL spectra excited by a 355 nm laser during decompression of the TXAN crystals (the " R " is the abbreviation of reverse).

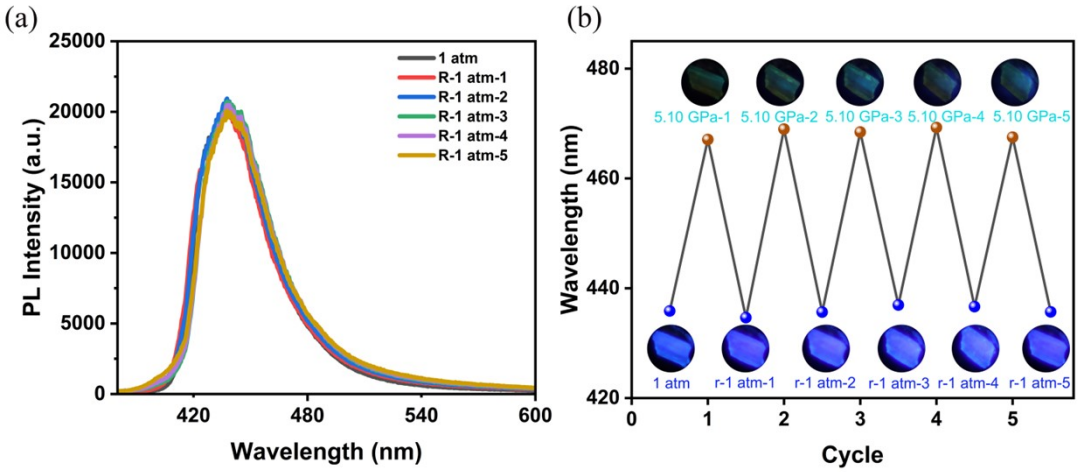

Figure S7. (a) PL spectra of TXAN reverses to 1 atm for 5 cycles. (the "R" is the abbreviation of reverse) (b) Wavelength and fluorescence photographs of pressurized to 5.10 GPa and depressurized to 1 atm for 5 cycles of TXAN. (the "r" is the abbreviation of reverse)

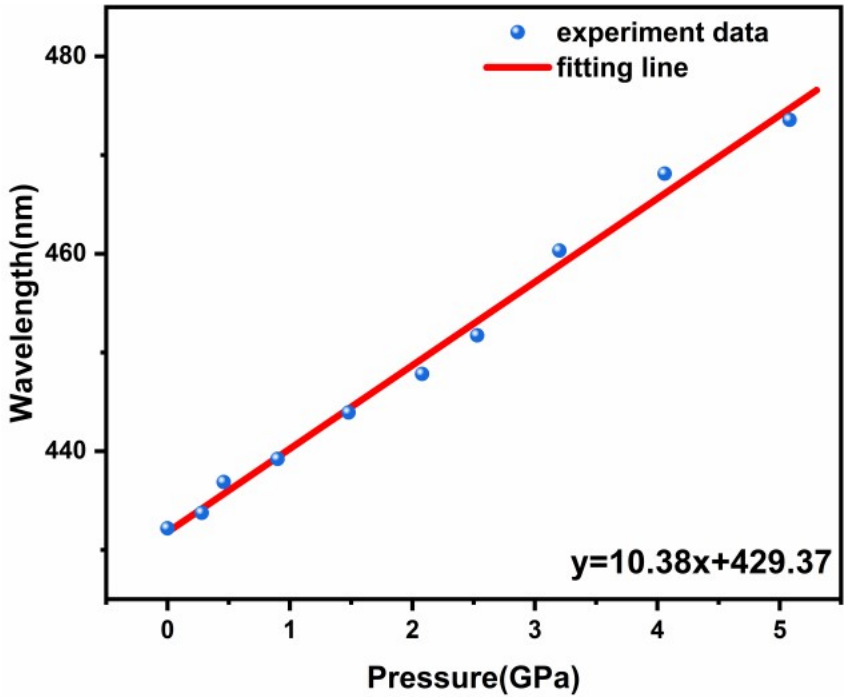

Figure S8. Emission peak position as a function of pressure.

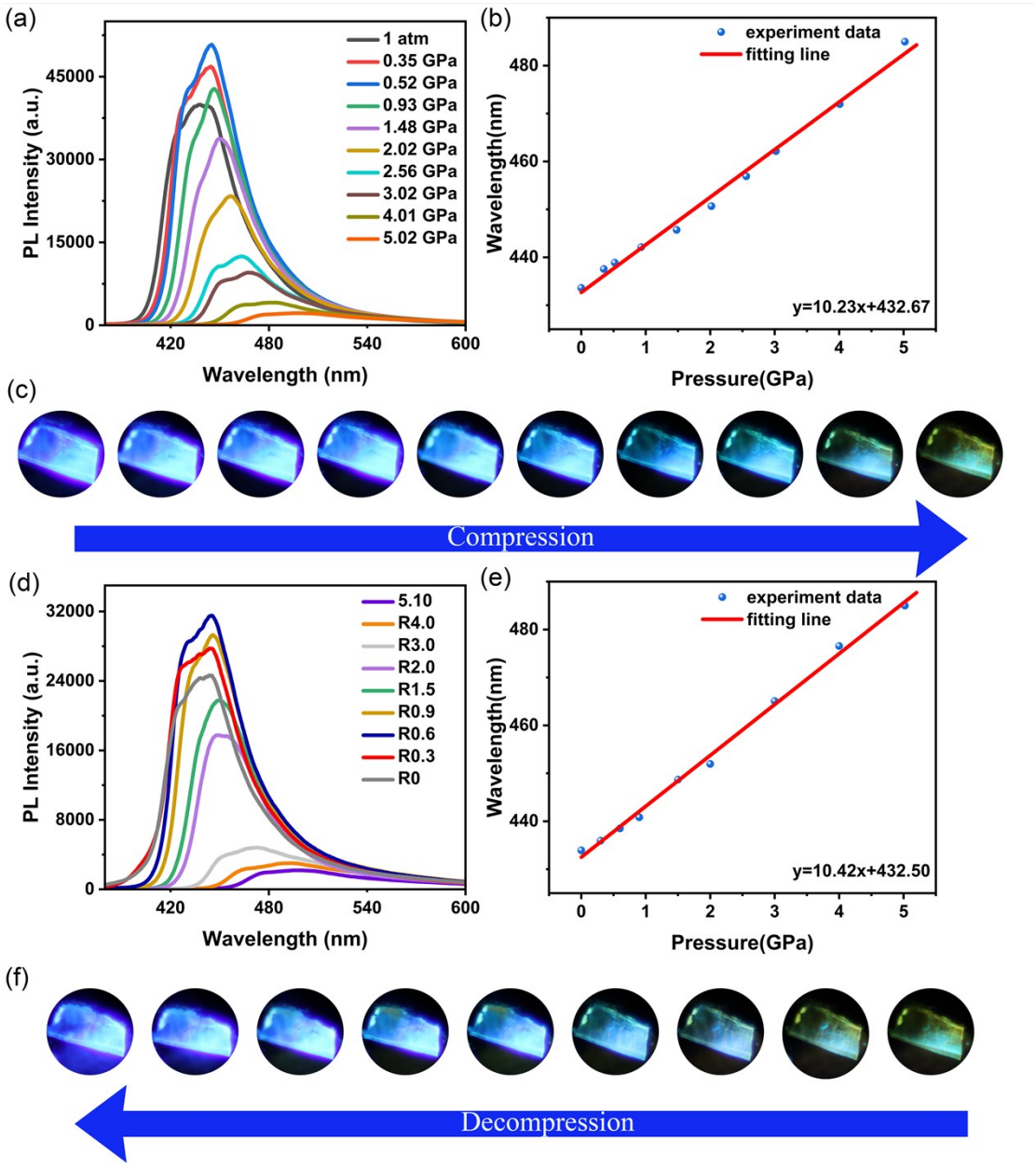

Figure S9. PL evolution of TXAN crystals under 355 nm excitation: (a) Pressurization and (d) Decompression. Emission maximum position of peak as functions of pressure: (b) Pressurization and (e) Decompression. Fluorescence images of the crystal: (c) Pressurization and (f) Decompression.

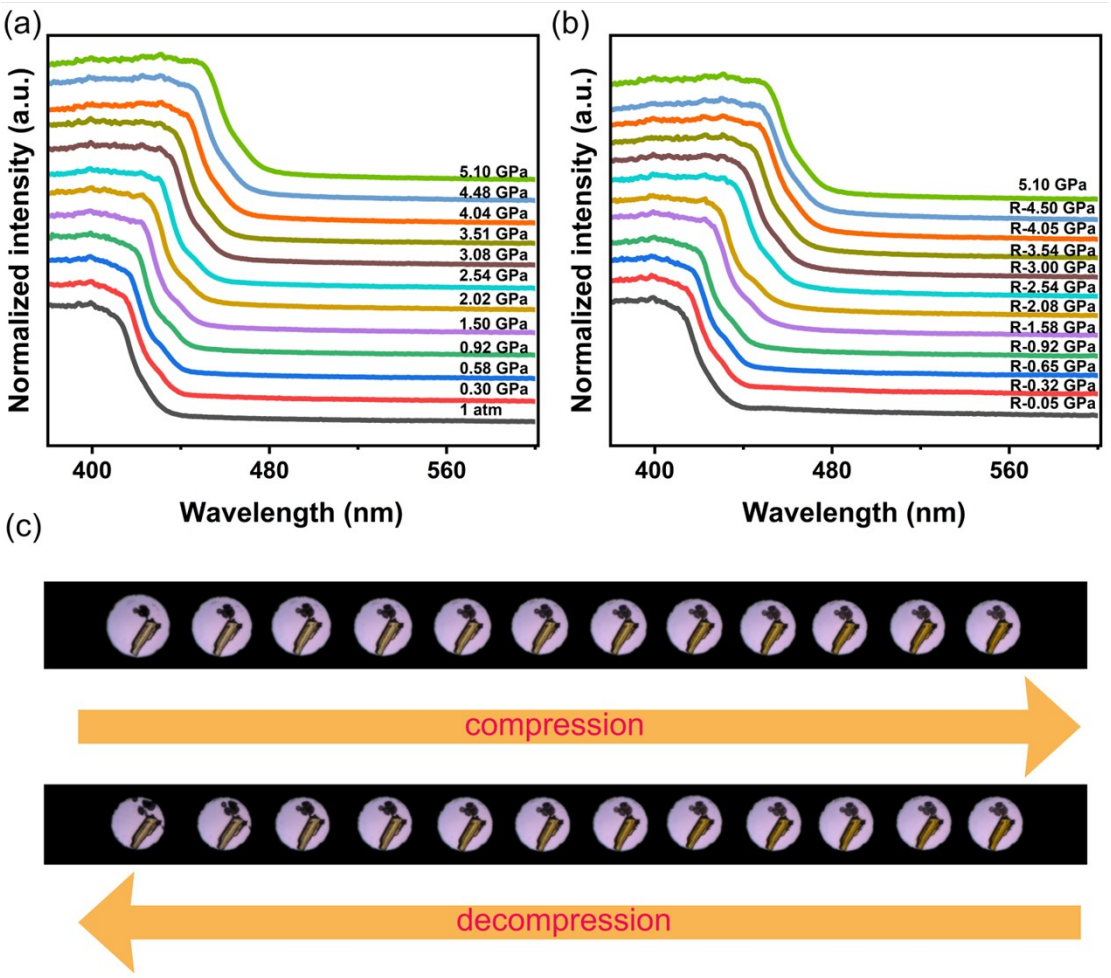

Figure S10. UV-visible absorption spectra (a) Pressurization and (b) Decompression of TXAN crystals at pressures up to 5.10 GPa. (the "R" is the abbreviation of reverse) (c) Images of normal photographs of the TXAN crystals.

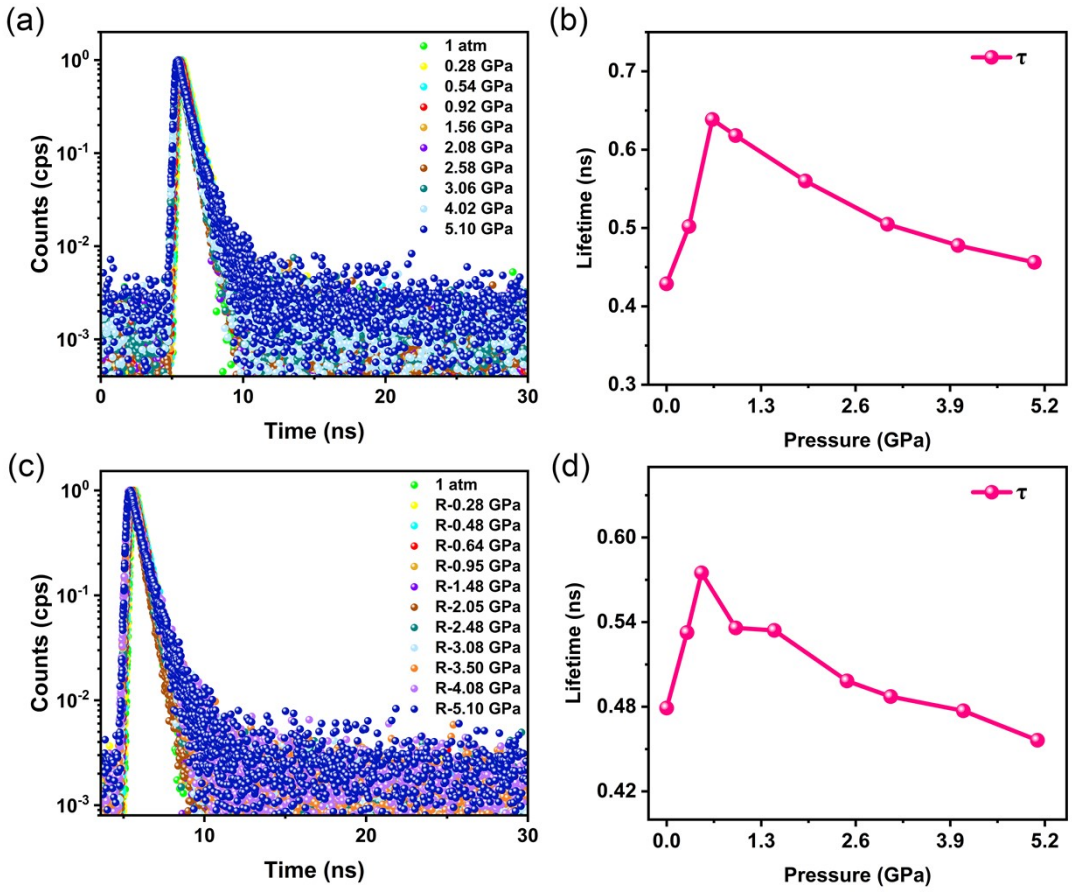

Figure S11. *In situ* high-pressure time-resolved PL spectra of TXAN crystals at various pressures: (a) Pressurization and (b) Decompression. Plots of fluorescence lifetime against pressure for the TXAN crystals: (c) Pressurization and (d) Decompression.

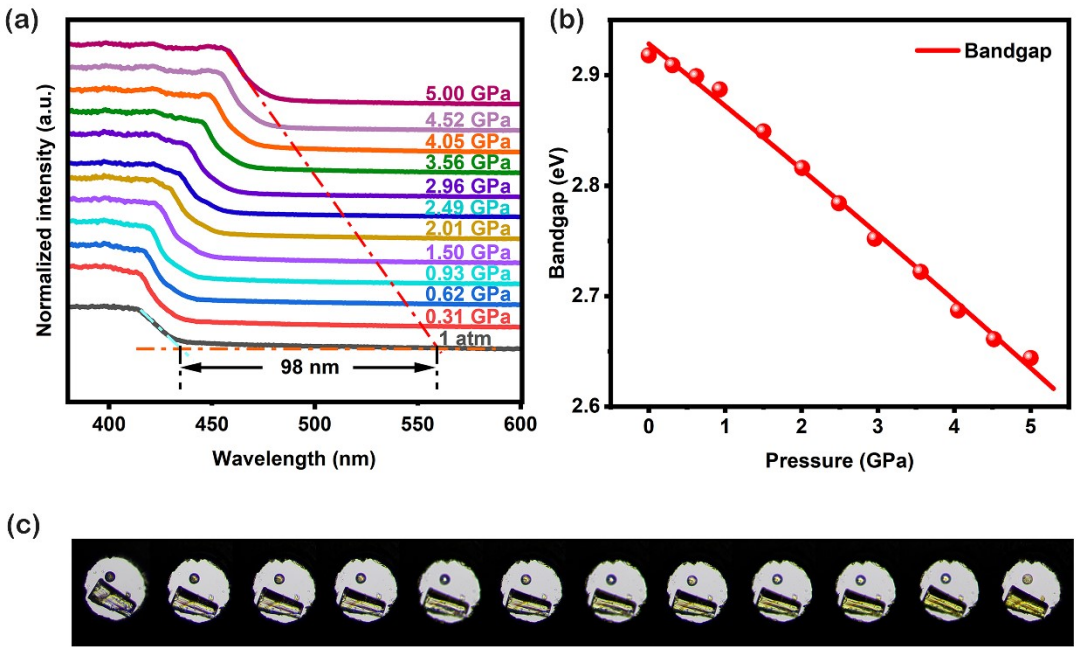

Figure S12. (a) UV-visible absorption spectra of the TXAN crystals at different pressures.

(b) Bandgap evolution of TXAN under high-pressure.

(c) Images of normal photographs of the TXAN crystals.

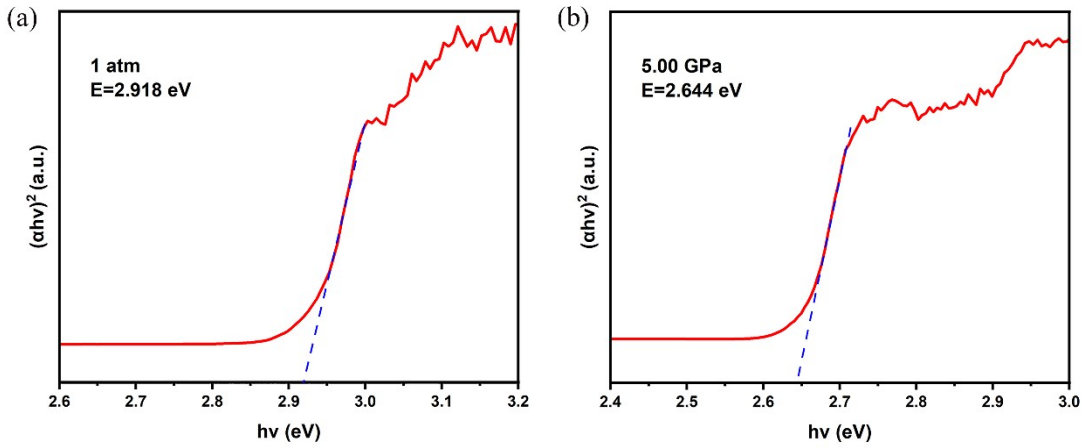

Figure S13. (a) Tauc plot for TXAN at 1 atm.

(b) Tauc plot for TXAN at 5 GPa.

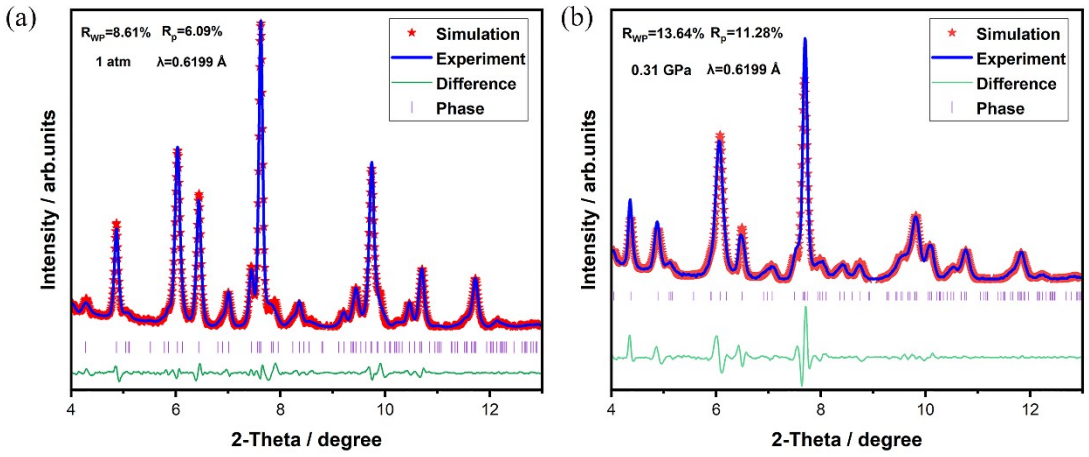

Figure S14. (a) Rietveld refinement of the pattern collected at 1 atm.

(b) Rietveld refinement of the pattern collected at 0.31 GPa.

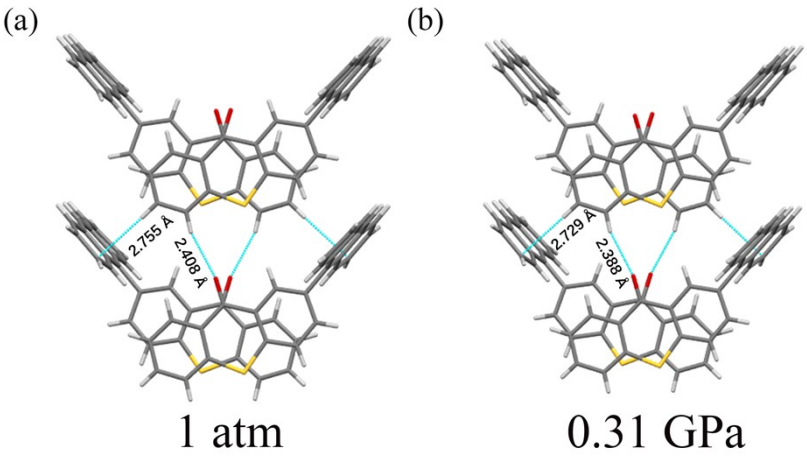

Figure S15. Pressure dependence of C–H···O and C–H···π interaction distances.

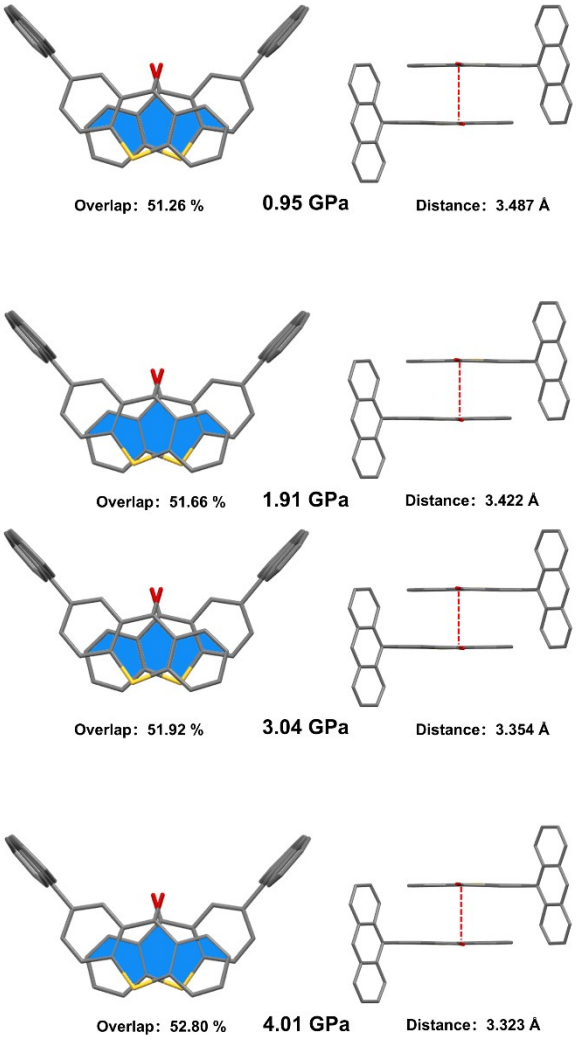

Figure S16. The stacking area and interplanar distance of the TXAN dimer under different pressures.

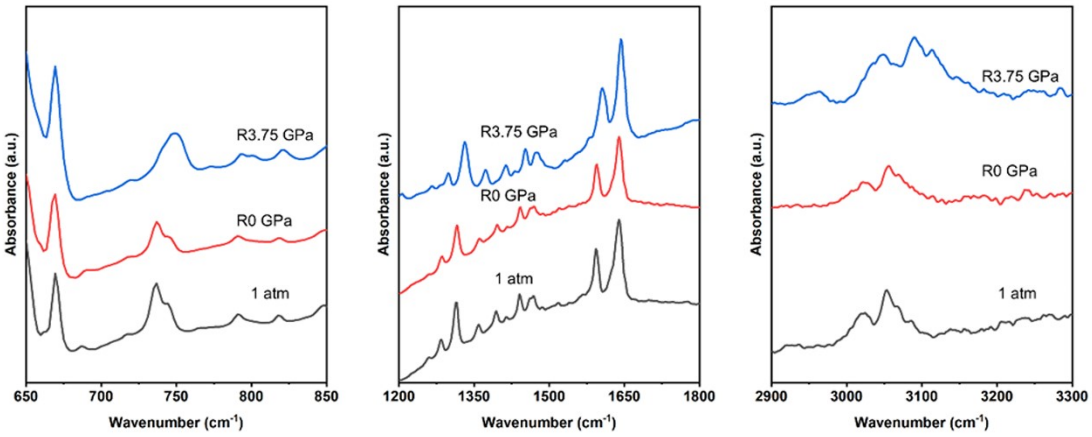

Figure S17. Decompression IR spectra of TXAN crystal (the " R" is the abbreviation of reverse).

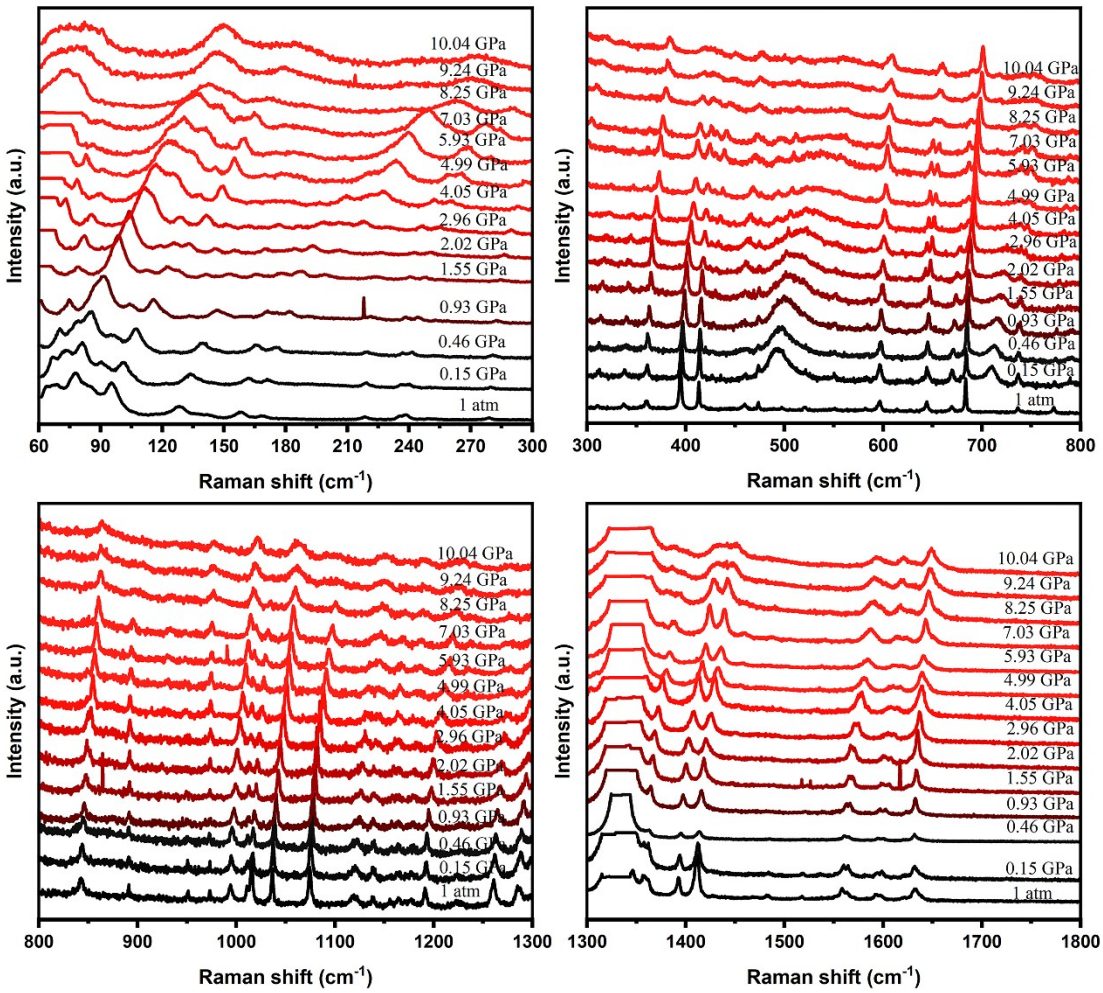

Figure S18. High pressure Raman spectra of TXAN crystal.

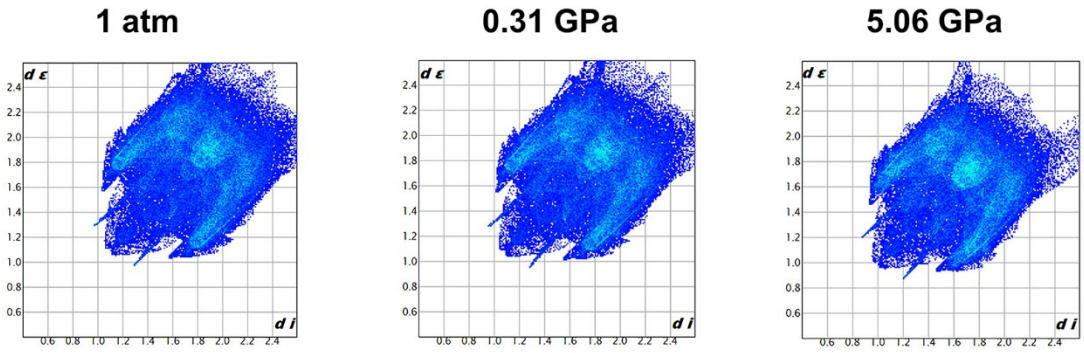

Figure S19. Fingerprint plot analysis of TXAN under different pressures.

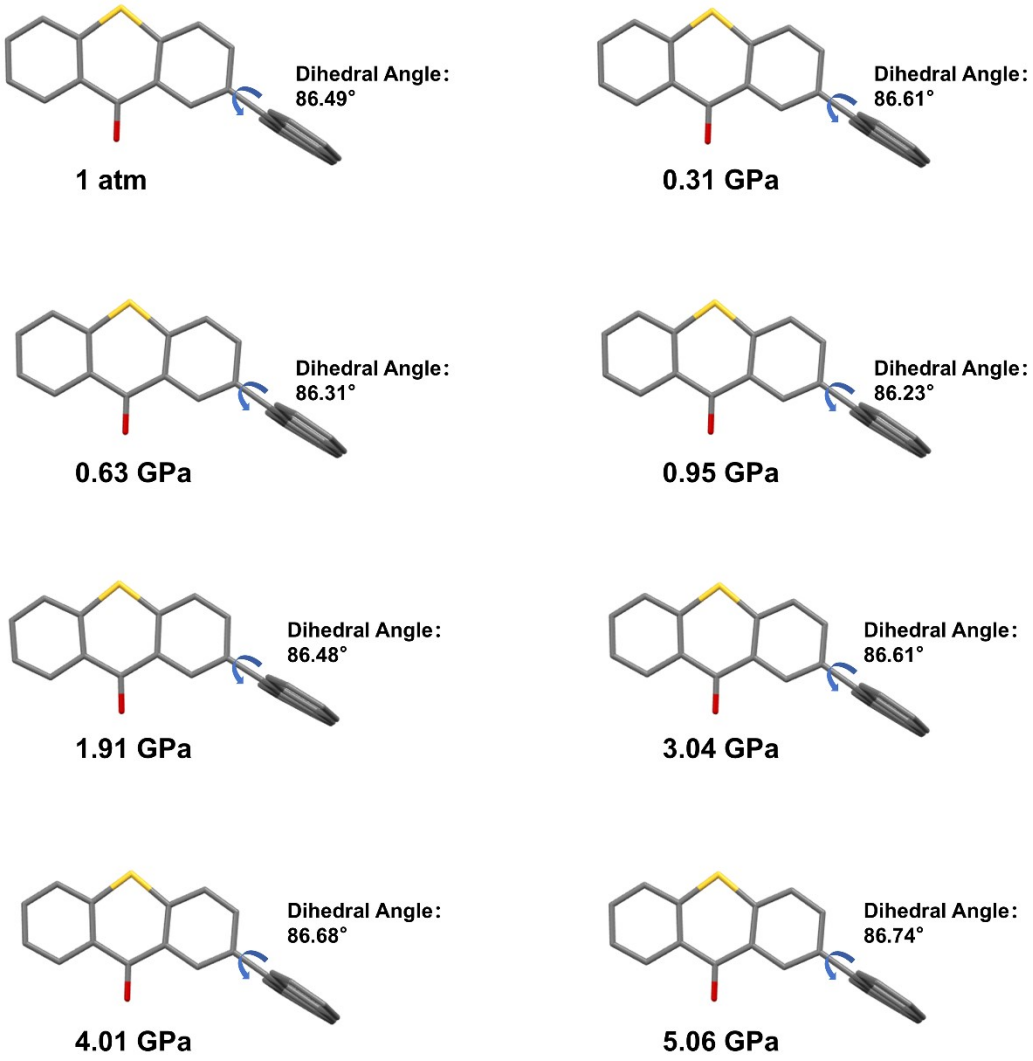

Figure S20. The dihedral angle of the TXAN dimer under different pressures.

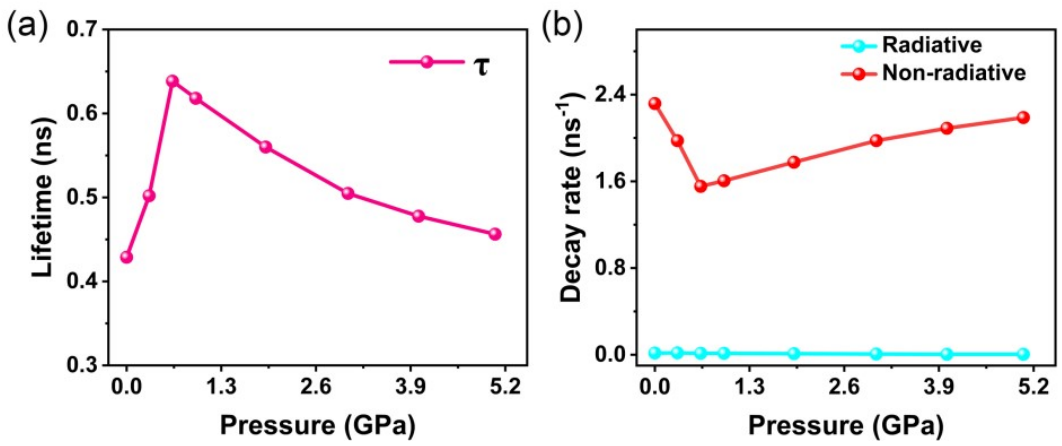

Figure S21. (a) Pressure-dependent evolution of the TXAN crystal lifetime. (b) Evolution of the radiative and nonradiative rate constants of the TXAN crystal with pressure.

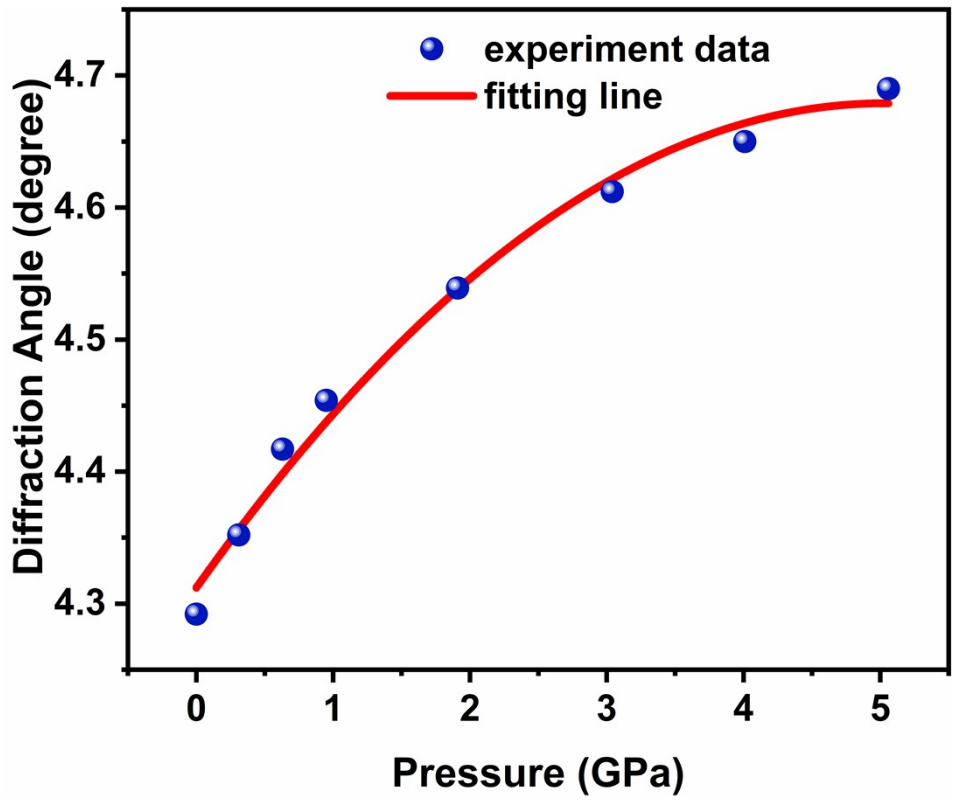

Figure S22. Variation of the (002) plane diffraction angle with pressure.

Reference

[1] Chen N H, Silvera I F. Excitation of ruby fluorescence at multimegabar pressures. Rev Sci Instrum 1996;67(12):4275-8.

[2] Payne M C, Teter M P, Allan D C, Arias T A, Joannopoulos J D. Iterative minimization techniques for ab initio total-energy calculations: molecular dynamics and conjugate gradients. Rev Mod Phys 1992;64(4):1045.

[3] Perdew J P, Burke K, Ernzerhof M. Generalized gradient approximation made simple. Phy Rev Lett 1996;77:3865-8.

[4] M. J. Frisch, G. W. Trucks, H. B. Schlegel, G. E. Scuseria, M. A. Robb, J. R. Cheeseman, G. Scalmani, V. Barone, G. A. Petersson, H. Nakatsuji, X. Li, M. Caricato, A. V. Marenich, J. Bloino, B. G. Janesko, R. Gomperts, B. Mennucci, H. P. Hratchian, J. V. Ortiz, A. F. Izmaylov, J. L. Sonnenberg, D. Williams-Young, F. Ding, F. Lipparini, F. Egidi, J. Goings, B. Peng, A. Petrone, T. Henderson, D. Ranasinghe, V. G. Zakrzewski, J. Gao, N. Rega, G. Zheng, W. Liang, M. Hada, M. Ehara, K. Toyota, R. Fukuda, J. Hasegawa, M. Ishida, T. Nakajima, Y. Honda, O. Kitao, H. Nakai, T. Vreven, K. Throssell, J. A. Montgomery, Jr., J. E. Peralta, F. Ogliaro, M. J. Bearpark, J. J. Heyd, E. N. Brothers, K. N. Kudin, V. N. Staroverov, T. A. Keith, R. Kobayashi, J. Normand, K. Raghavachari, A. P. Rendell, J. C. Burant, S. S. Iyengar, J. Tomasi, M. Cossi, J. M. Millam, M. Klene, C. Adamo, R. Cammi, J. W. Ochterski, R. L. Martin, K. Morokuma, O. Farkas, J. B. Foresman, and D. J. Fox, *Gaussian 16 Rev. C.01*, Wallingford, CT, **2016**.